A Modeling Study of the Interannual Variability in the Wintertime North Atlantic Ocean*

D. S. BATTISTI

Department of Atmospheric Sciences, University of Washington, Seattle, Washington

U. S. BHATT

Department of Atmospheric and Oceanic Sciences, University of Wisconsin-Madison, Madison, Wisconsin

M. A. ALEXANDER

CIRES, University of Colorado, Boulder, Colorado

(Manuscript received 1 September 1994, in final form 15 May 1995)

ABSTRACT

A new model for the upper North Atlantic Ocean is presented and used to hindcast the SST from 1950 to 1988. The model consists of a matrix of one-dimensional (independent) columns in which a variable-depth, bulk mixed layer overlies a diffusive convective thermocline. The climatological annual cycle of heat flux convergence by the oceanic circulation is implicitly included in the formulation of the forcing. The 39-yr control integration of the model includes as surface forcing the shortwave and net longwave radiation from a control integration of the community climate model. Sensible and latent heat fluxes are determined from instantaneous values of surface temperature, humidity, and wind speed from the atmospheric model, and the SST simulated by the ocean model using the bulk formulae. The hindcast is performed by repeating the control integration, adding the observed, monthly mean surface anomalies in surface temperature, humidity, and wind speed for the period 1950–88. Thus, the simulated SST anomalies are generated explicitly by anomalies in the latent and sensible heat fluxes. A separate hindcast integration is presented, using as forcing the "observed" sensible plus latent heat flux anomalies rather than the surface atmospheric field anomalies to demonstrate that the major results are not predetermined by the formulation of the coupling.

The ability of the model to hindcast the wintertime interannual variations in SST is demonstrated by simple correlations with observed anomalies and by comparing the composite of warm and cold events observed with those simulated by the model. There is a good quantitative agreement between simulated and observed SST anomalies throughout most of the North Atlantic Ocean. Since the model formulation explicitly excludes any effects due to *anomalies* in the ocean advection, our results confirm the hypothesis that wintertime interannual to subdecadal variability in SST is mainly due to local anomalies in the air–sea flux of sensible and latent heat and not to anomalies in oceanic advection. Significant disagreement between hindcast and simulated SST anomalies is limited to a small region extending from Cape Hatteras to Nova Scotia along the U.S. coast. Here, the observed surface flux anomalies are anticorrelated with the SST anomalies, implicating important changes in oceanic advection in the generation of interannual wintertime SST and surface flux anomalies.

Both the sensible and latent heat flux anomalies are shown to contribute substantially to the wintertime anomalies in SST in the subpolar Atlantic, while the heat flux anomalies are predominantly determined by the latent heat flux in the subtropics. Entrainment anomalies contribute to a lesser extent to the mixed layer temperature anomalies throughout the basin. Sensitivity studies are performed to highlight the atmospheric processes and variability that account for the surface heat flux anomalies.

1. Introduction

Bjerknes (1964) was the first to document the dominant concurrent patterns of interannual variability in the wintertime North Atlantic sea surface temperature (SST) and sea level pressure (SLP). More recently, Kushnir (1994) presented composites of the "warm minus cold" wintertime (December–April mean) climate anomalies in the North Atlantic on the interannual timescales. Kushnir's results, obtained from a much larger dataset, confirmed the earlier results of Bjerknes. The surface signature of the warm phase of this dominant pattern of variability is displayed in Fig. 1. North of 40°N, anomalously warm water is associated with anomalously high SLP, warm air, and reduced westerly

* Joint Institute for the Study of the Atmosphere and Oceans Contribution Number 256.

Corresponding author address: Dr. David S. Battisti, Dept. of Atmospheric Sciences, AK-40, University of Washington, P.O. Box 351640, Seattle, WA 98195-1640.

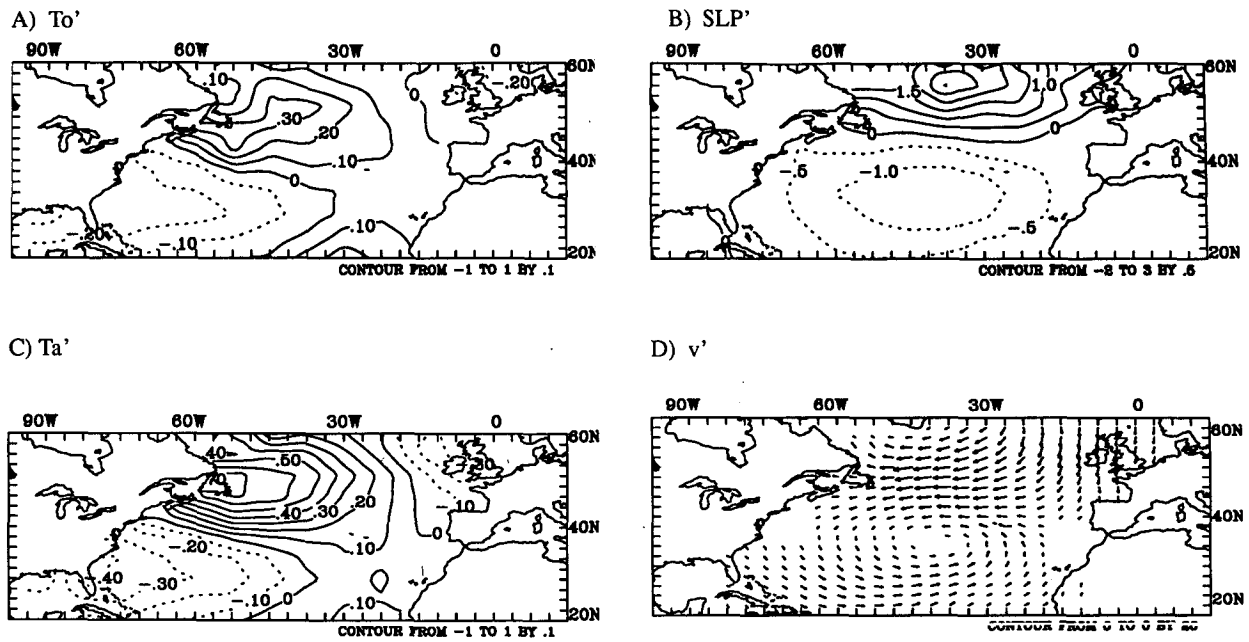

FIG. 1. A composite of observed wintertime (November to April) interannual "warm" events in the North Atlantic. (a) SST anomaly (contour interval, c.i., is 0.1°C); (b) sea level pressure, in mb; (c) surface air temperature anomaly, T_a' (c.i. 0.1°C); (d) surface wind vector anomaly. The observations are from the Comprehensive Ocean–Atmosphere Data Set (COADS). The years that constitute the composite are listed in Table 1. Solid contours are positive.

winds. Concurrent with the anomalously warm water in the northern basin, cold water is found to the south (20°–30°N) where the SLP is anomalously low and the surface air is cold. The cold phase of this dominant "mode" is essentially the negative of Fig. 1.

Bjerknes argued that these interannual climate anomalies are the result of the interaction between the atmosphere and the ocean. Specifically, he argued that local thermodynamic processes in the atmosphere and the ocean are important for interannual climate anomalies and that the response of the ocean is confined to the upper ocean. Wallace et al. (1990) and Wallace et al. (1992) present EOF and singular value decomposition analyses, respectively, that link the wintertime pattern of SST anomalies in the North Atlantic with anomalies in the 500-mb height field (Z500). Wallace et al. (1990) determined that the relationship between the anomalies in Z500 and in the SST tendency is stronger than that between the anomalies in Z500 and those in SST. This result is consistent with the hypothesis that on the interannual timescale the dominant thermodynamic processes in the surface ocean are due to local air–sea exchanges. Wallace and Jiang (1987), using lag-correlation analysis, found that the correlations between Z500 and SST anomalies were largest with Z500 anomalies leading the SST anomalies. Davis (1976) and Lanzante (1984) came to similar conclusions using the same analysis technique on the SST with the SLP and Z700, respectively. Together, these studies indicate that the atmospheric anomalies lead the SST anomalies by one to several months, suggesting that the dominant coupled atmosphere–ocean mode, first identified by Bjerknes, is at least initiated by atmospheric circulation anomalies. Furthermore, all of the above studies indicate that the horizontal scale of the SST anomalies is governed by the scale of the associated atmospheric circulation anomalies and not by the synoptic-scale oceanic eddies.

Haney (1985) argued that *local* surface heat flux anomalies are responsible for the interannual SST anomalies in the midlatitude Pacific Ocean, after demonstrating the anomalies in oceanic advection cannot account for the amplitude of the observed SST anomalies. In the midlatitudes during winter, the important surface heat flux anomalies are the sensible (Q_S) and latent (Q_L) fluxes: the variance in the shortwave and longwave radiation (and in the net radiation) is small compared with the turbulent transfer of heat (see, e.g., Cayan 1992a). Cayan (1992b) performed an analysis of the interannual variability in the SLP and in the anomalous sensible plus latent heat flux (Q_{S+L}), averaged monthly during the wintertime in the North Atlantic. He found that the predominant EOF of SLP anomalies, the North Atlantic Oscillation (NAO) (van Loon and Rogers 1978), is associated with large-scale Q_{S+L} anomalies. Specifically, in one phase of the NAO, an anomalous zonal band of positive heat flux into the ocean at about 50°N is associated with anomalous high

SLP to the north. Concurrently, between about 30° and 40°N, a broad region of low pressure associated with the NAO overlies anomalous negative Q_{S+L}. In a follow-up study, Cayan (1992b) presented a composite of the occurrences of the extreme in the index of the NAO and demonstrated that the month-averaged wintertime Q_{S+L} anomalies are consistent with the observed anomalous SST tendency.

In this study we test the hypothesis that the interannual wintertime SST anomalies in the North Atlantic are primarily governed by the local ocean-to-atmosphere energy fluxes and are primarily confined to the upper ocean. To this end, we employ a model of the upper ocean in the North Atlantic, described in section 2, that emphasizes the physics of the mixed layer and implicitly includes the effects of the annual cycle in ocean circulation on the annual cycle of SST. Furthermore, in the model formulation we have assumed that *anomalies* in the circulation of the ocean are, in general, not important for the wintertime anomalies in SST on the interannual timescale. We report in section 3 the results from a hindcast simulation of the upper North Atlantic Ocean response to prescribed observed anomalies in the atmospheric surface variables. The resultant "sensible plus latent" heat flux (Q_{S+L}) anomalies are calculated using standard bulk formulae and are dependent on the SST calculated from the interactive ocean model. The results are presented in composite form as in Kushnir (1994). Specifically, we composite the simulated SST anomalies for 10 winters (defined as the November–April mean) when the observed SST was anomalously high in the far northern Atlantic; a cold event composite is also presented. The simulated anomalies in SST and heat flux are compared with the SST and heat flux anomalies obtained from a composite of the observations using the same winters. The importance of the anomalies in surface air temperature, wind speed, and humidity in determining the total heat flux Q_{S+L} is examined in section 4. A discussion is found in section 5, and conclusions are presented in section 6.

Finally, our interest in this study is on SST anomalies on the interannual to subdecadal timescale, hereafter referred to broadly as the "interannual" timescale. Hence, throughout the paper we apply a high-pass digital filter (with a 10-yr half-power point) to all observed fields and to the flux anomalies (estimated from the unfiltered data and using the bulk formulae).

2. The ocean model and experimental design

The central hypotheses we are testing in this study is that the interannual variability in wintertime SST anomalies in the North Atlantic Ocean is determined by processes that are inherently associated with local atmosphere–ocean coupling, and the important physics and thermodynamics responsible for these climate anomalies are confined to the mixed layer: we assume changes in SST due to ocean dynamics (advection) become important only for longer timescale (decadal or more) fluctuations. Therefore, we employ an ocean model that has a detailed representation of the mixed layer physics and explicitly excludes deep ocean physics. The advantages of this model over an oceanic GCM include: the model is relatively easy to diagnose, is computationally efficient, and does not require lengthy integrations to obtain a statistically steady state.

a. The ocean model

The ocean model is designed to study the influence of atmospheric forcing and entrainment on SSTs in the North Atlantic Ocean. The ocean model grid, which is aligned with the NCAR Community Climate Model (CCM1) grid between 20° and 60°N in the Atlantic, is composed of horizontally independent column models of the upper ocean. The upper-ocean model includes prognostic mixed layer physics and, below the mixed layer and through the permanent thermocline, a convective–diffusive model.

A well-mixed surface layer is assumed a priori. The temperature of the mixed layer T_{om} is controlled by vertical processes including surface energy fluxes, penetrating solar radiation, and entrainment. The salinity in the mixed layer is a time-dependent model variable and is contingent upon precipitation and evaporation at the surface and entrainment and diffusion at the base of the mixed layer. The mixed layer depth h is computed using the formulation of Gaspar (1988) and is a time-dependent variable. The mixed layer depth depends on the surface buoyancy forcing, wind stress, penetrating solar radiation, and the density jump at the base of the mixed layer. Under stable conditions, the mixed layer will re-form closer to the surface: entrainment is set to zero, and h is computed diagnostically by assuming a balance between turbulent kinetic energy generation, buoyancy forcing, and dissipation. When the mixed layer shallows, the temperature and salinity profiles are adjusted according to Adamec et al. (1981), conserving heat, salt, and potential energy.

Beneath the mixed layer, heat and salt are affected by convective overturning and vertical diffusion. A Laplacian formulation is used for the vertical diffusion of temperature and salinity: a constant eddy diffusion coefficient of 2×10^{-5} m^2 s^{-1} is used, based on the study of White and Walker (1974) (see also Alexander and Deser 1995). The absorption of solar radiation is also included in the convective/diffusive region below the mixed layer using the parameterization of Paulson and Simpson (1977). The convective–diffusive model contains 30 unequally spaced layers between the surface and 1000-m depth; the values of the state variables in the layers within the mixed layer are equal to the mixed layer values. Thirteen of the layers are within the first 100 m to resolve the sharp summer pycnocline. The temperature of water below the mixed layer, used

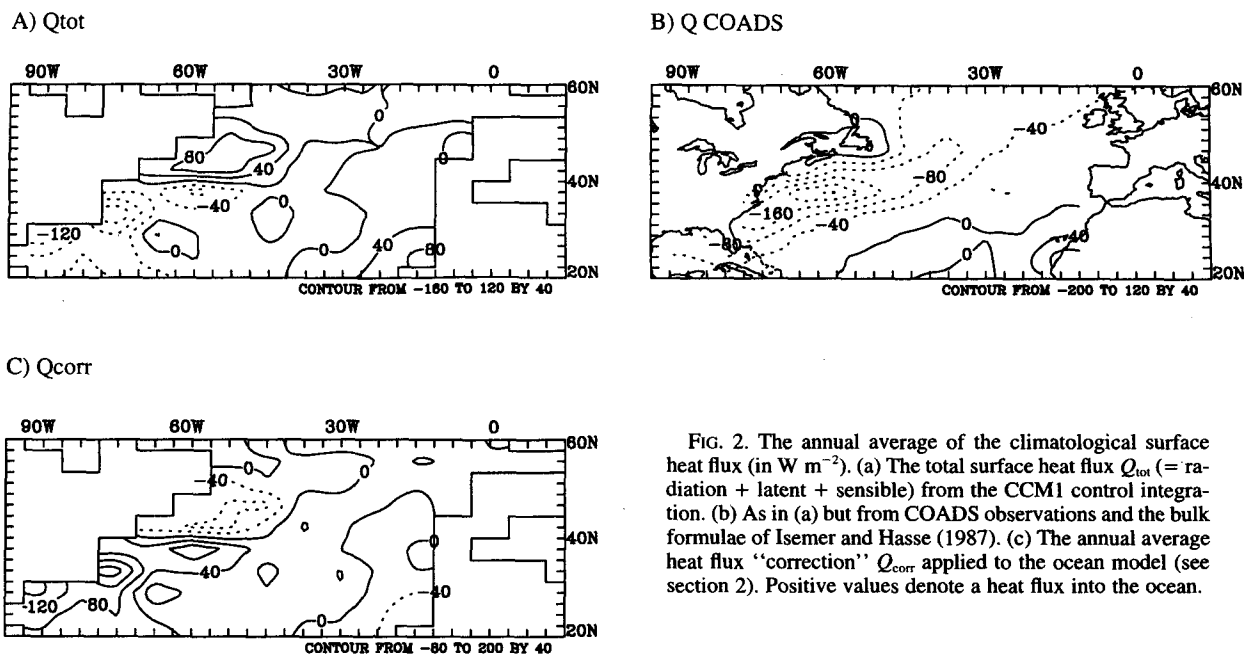

FIG. 2. The annual average of the climatological surface heat flux (in W m^{-2}). (a) The total surface heat flux Q_{tot} (= radiation + latent + sensible) from the CCM1 control integration. (b) As in (a) but from COADS observations and the bulk formulae of Isemer and Hasse (1987). (c) The annual average heat flux "correction" Q_{corr} applied to the ocean model (see section 2). Positive values denote a heat flux into the ocean.

in the entrainment calculations, is obtained directly from the layer in which h resides.

A similar version of the column model has been used by Alexander and Deser (1995) to simulate the thermal structure of the upper ocean at several locations in the North Atlantic and the North Pacific. A more detailed description of the column model is given in the appendix.

b. *Coupling to the atmospheric fields*

The formulation of the coupling of the ocean model to atmospheric variables anticipates future studies in which the ocean model will be interactively coupled to an atmospheric GCM, the CCM1. Net surface fluxes into the ocean are determined using daily values of the surface atmospheric fields obtained from a 5-yr control run of the CCM1 (R15, case 256 of Williamson et al. 1987). In this control CCM1 integration, the SST is prescribed to be the observed annual cycle from the Alexander and Mobley (1976) dataset. The ocean model is forced with the daily values of the net radiative flux, the momentum flux, the "latent + sensible" Q_{S+L} heat flux, and the precipitation minus evaporation flux. The radiation and momentum fluxes are from the CCM1 control integration (with prescribed climatological SST). The Q_{S+L} and the momentum fluxes are determined from the bulk formulae using the prescribed atmospheric variables from the history tapes of the CCM1 control run and the *simulated* SST: the (bulk) flux formulae that are used in calculating Q_{S+L} are identical to that in the CCM1 (Deardorff 1972).

The ocean model, being composed of a matrix of independent mixed layer models, does not explicitly account for the horizontal advection of heat in the ocean. Thus, when forced by the total surface heat flux Q_{tot} (latent + sensible + radiative), the model will not produce a realistic seasonal cycle in regions where surface temperature advection is important (but see section 2c). To achieve an accurate seasonal cycle in SST, we have introduced a correction to the observed surface heat flux in tuning the model (see, e.g., Sausen and Ponater 1988). This correction is obtained as follows. The ocean model is integrated for one time step (say from t_1 to t_2) with the forcing determined as stated in the previous paragraph. The simulated SST at t_2 is, in general, not equal to the observed climatological temperature at t_2. A heat flux correction Q_{corr} is then calculated as the additional heat that is required to achieve a surface mixed layer temperature equal to the climatological SST at t_2. The Q_{corr} is then stored and the simulated SST is set to the climatological value. The integration is continued for six years with a Q_{corr} calculated for each day using the (annually cycled) surface atmospheric fields from the first year of the CCM1 control run. Using the daily values of Q_{corr} from the last five years of this integration,[1] a monthly mean climatology of Q_{corr} is assembled. Hence, there are approximately 30*5 daily values of Q_{corr} that go into one monthly average.

[1] Since the initial conditions of the mixed layer model are necessarily inconsistent with the atmospheric fields, throughout year one a significant contribution to Q_{corr} results solely from this imbalance and not due to neglected ocean physics or the parameterization of the mixed layer physics. Hence, values of Q_{corr} from the first year of integration are not included in calculating the climatological Q_{corr}.

We repeat this procedure using surface data from *each* of the 5 years in the control CCM1 integration. Thus, we obtain 5 monthly estimates of Q_{corr}, which are then averaged to obtain the monthly average Q_{corr} that is stored and used in all simulations discussed hereafter. Note that Q_{corr} is applied at each ocean model time step (one day): the value of Q_{corr} is calculated for each day using a cubic spline from the monthly mean Q_{corr}. In all the integrations performed below, Q_{corr} has a fixed annual cycle that is independent of the state of the ocean or the atmosphere. The ocean model is henceforth forced at each basin grid point with the net heat flux:

$$Q_{net} = Q_L(q_a, V_a, T_{om}) + Q_S(T_a, V_a, T_{om}) + Q_{SW} + Q_{LWnet} + Q_{corr}(t) \quad (1)$$

$$Q_{net} \equiv Q_{tot} + Q_{corr}. \quad (2)$$

In Eq. (1), Q_L (Q_S) is the latent (sensible) heat flux, Q_{SW} is the surface shortwave flux into the ocean, Q_{LWnet} is the net longwave radiative flux at the surface, T_a is the temperature of the air at the lowest model level (at $\sigma = 0.991$), T_{om} is the SST from the ocean model, t is time, V_a is the speed of the surface wind, and Q_{tot} ($= Q_{net} - Q_{corr}$) is the sum of all the surface heat flux terms.

c. *Interpretation of Q_{corr}*

We note that *if* the surface energy fluxes that are simulated in the CCM1 were identical to the actual energy fluxes and our ocean basin model accurately represented the physics of the mixed layer, Q_{corr} would represent the horizontal heat flux convergence in the mixed layer due to ocean currents, which are neglected in the model. One anticipates that the heat flux convergence due to the ocean gyre currents should warm (cool) in the northern (southeastern) North Atlantic Ocean.

The calculated Q_{corr}, averaged over the year, is displayed in Fig. 2c. Throughout the paper, a positive heat flux represents a warming of the water in the mixed layer. The heat flux correction, required for the model to simulate the annual cycle, does not resemble the advective oceanic heat flux convergence (allowing for uncertainties in the surface heat flux, the heat flux convergence will be very similar to the negative of Fig. 2b). In fact, Q_{corr} is primarily due to errors in the surface energy fluxes in the control integration of the CCM1 and to neglected advective effects. The former errors result from errors in the atmospheric model, especially the shortwave radiation incident at the ocean surface, and yield an overestimate of the surface warming (in this case off the northeast United States and eastern Canadian coasts) in the subpolar oceans (cf. Figs. 2a and 2b). This is a common problem in many atmospheric GCMs and stems from an insufficient amount of low-level cloud (e.g., Soden 1992). We note that the calibration of the ocean model was also performed using the "observed" surface fluxes from the COADS long-term mean (Fig. 2b), avoiding the problematic Q_{SW} in the CCM1. In this case, Q_{corr} does indeed have the pattern and amplitude that is consistent with what one would expect from the oceanic flux convergence. Since the ultimate goal of our work is not to provide a hindcast of the SST but to examine the interactive atmosphere–ocean coupled system, we develop the ocean model with Q_{corr} based on the CCM1 climatological fields.

d. *The control integration of the ocean model*

The control integration is for 39 years, whereby the ocean model is forced using (1) and the 5 years of daily atmospheric variables from the CCM1 control integration (prescribed cyclically). The initial conditions for the control integration were obtained from the end state of an extended ocean model control integration, forced by the CCM1 net surface flux. The climatological SST from the control run of the model is very close to the observed climatology; the drift in simulated SST is less than 0.1°C over 30 years, except for two isolated grid points approaching 0.17°C/30 yr, indicating a stable simulation. However, the variance in the simulated wintertime SST from the ocean control integration is about one-half of that from the observations.

3. The response of the upper North Atlantic Ocean to the observed (prescribed) surface atmospheric conditions

a. *The hindcast*

In this section we report on the hindcast of the upper North Atlantic Ocean response to the observed state of the atmosphere from 1950 to 1988 using the ocean model described in section 2. The model is forced as follows: the observed monthly averaged anomalies in the surface atmospheric air temperature T'_a, the surface specific humidity q'_a, and the average of the instantaneous wind speed V'_a (averaged over the month) are added to the surface atmospheric fields used in the 39-yr control integration of the ocean model (i.e., added to the daily values of T_a, V_a, and q_a from the control integration of the CCM1). The resulting fields are then used to calculate the net heat flux forcing of the ocean model:

$$Q_{net} = Q_L(q_a + q'_a, V_a + V'_a, T_{om}) + Q_S(T_a + T'_a, V_a + V'_a, T_{om}) + Q_{SW} + Q_{LWnet} + Q_{corr}(t). \quad (3)$$

These atmospheric anomaly data, denoted by ($'$), are taken from the Comprehensive Ocean–Atmosphere Data Set (COADS). The atmospheric anomalies are determined using the long-term monthly mean climatological annual cycle from COADS. In (3), T_{om} is the

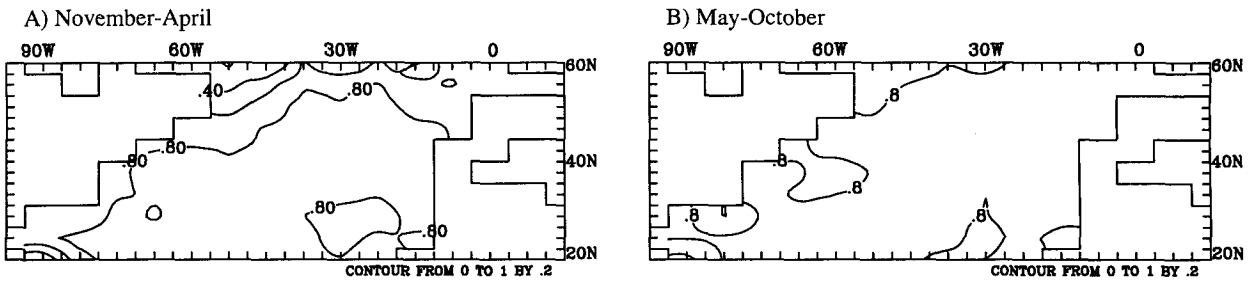

FIG. 3. The correlation coefficients for the observed with the hindcast SST anomaly during (a) winter and (b) summer. Winter (summer) is defined as the November through April (May through October) mean. The integration spans 1950–88.

actual SST (also the mixed layer temperature) from the evolving mixed layer model. Finally, a digital filter (10-yr half-power point) is applied to the 39-yr record of anomalies to remove the very low frequency (subdecadal) variability.

The total flux forcing in the model hindcast is calculated using (3), where the bulk formulae for calculating the sensible and latent heat fluxes are exactly those used in the CCM1. The thermodynamic forcing of the ocean model is explicitly limited to anomalies in Q_{S+L}: the radiative fluxes (Q_{SW}) and Q_{corr} are identical to that in the control integration. The observed anomalies in the momentum flux are also imposed on the ocean model in the hindcast. Due to insufficient observations, however, there are no anomalies in precipitation.

A partial measure of the skill of the model is provided by the correlation of the model hindcast SST anomaly with that observed (from COADS). Displayed in Fig. 3 are maps of the correlation coefficient based on the monthly mean anomalies for the summer (May–October) and winter (November–April) seasons. The correlation coefficients for the hindcast with the observed SST anomalies generally exceed 0.8 for both the 3 and 6 month (seasonal) average anomalies.[2] Weaker correlations are found in isolated regions in the northwest extremity of the domain and to the west of the Canary Islands (Fig. 3), where the observational database is relatively sparse. The correlation coefficient is statistically significant at the 99% level almost everywhere in the domain: this criteria is not met in the winter semester for some of the grid points along the northern border of the domain in winter where sea ice, ignored in this study, is observed (see Fig. 3a).

The results of the hindcast in composite form are presented. The years that constitute a composite event are determined in the following manner. An index was formed based on the difference in the wintertime (November to April average) SST anomaly between 40°–60°N and 20°–40°N. The index is chosen based on the EOF analysis of SST throughout the Atlantic basin, which features a first mode that has a zonally oriented dipole pattern in SST, with centers of opposite polarity in these two regions (see, e.g., Wallace et al. 1990). The 20 extreme values of this index (10 of each polarity) define the years that constitute the warm and cold composite events, and are listed in Table 1. These years are not strictly a subset of those identified and included in the composites of Kushnir (1994). Kushnir notes that the nature of the composite events is insensitive to the number of cases and specific years that go into the composite. We confirm this conclusion for the composites obtained from the hindcast (not shown).

The composite of the *observed* events are displayed as anomalies from the climatological mean. Specifically, the anomalies in the atmospheric quantities, in the SST, and in the "observed" Q_{S+L} anomalies are based on the observed climatological means from COADS (1950–88); the bulk flux formulation is the same as that used in the CCM1 (Deardorff 1972). All anomalies are filtered to remove the low frequency (decadal) variability.

For the events that compose the hindcast (simulated) composites (see Table 1), the model SST and mixed layer depth anomalies are calculated by subtracting time series of the variable obtained in the ocean model

TABLE 1. The years that define the warm and cold composite events. Years that do not appear in Kushnir's composite events are indicated by (*).

Warm event	Cold event
1950–51	1953–54*
1952–53	1956–57*
1954–55	1958–59
1957–58	1960–61
1964–65	1971–72
1965–66	1972–73
1967–68	1973–74
1968–69*	1974–75
1969–70	1979–80*
1980–81	1985–86

[2] Correlations generally exceed those presented in Luksch (1995), possibly because the latter correlations are based on the monthly anomalies for January while those presented here are for the seasonal mean anomalies.

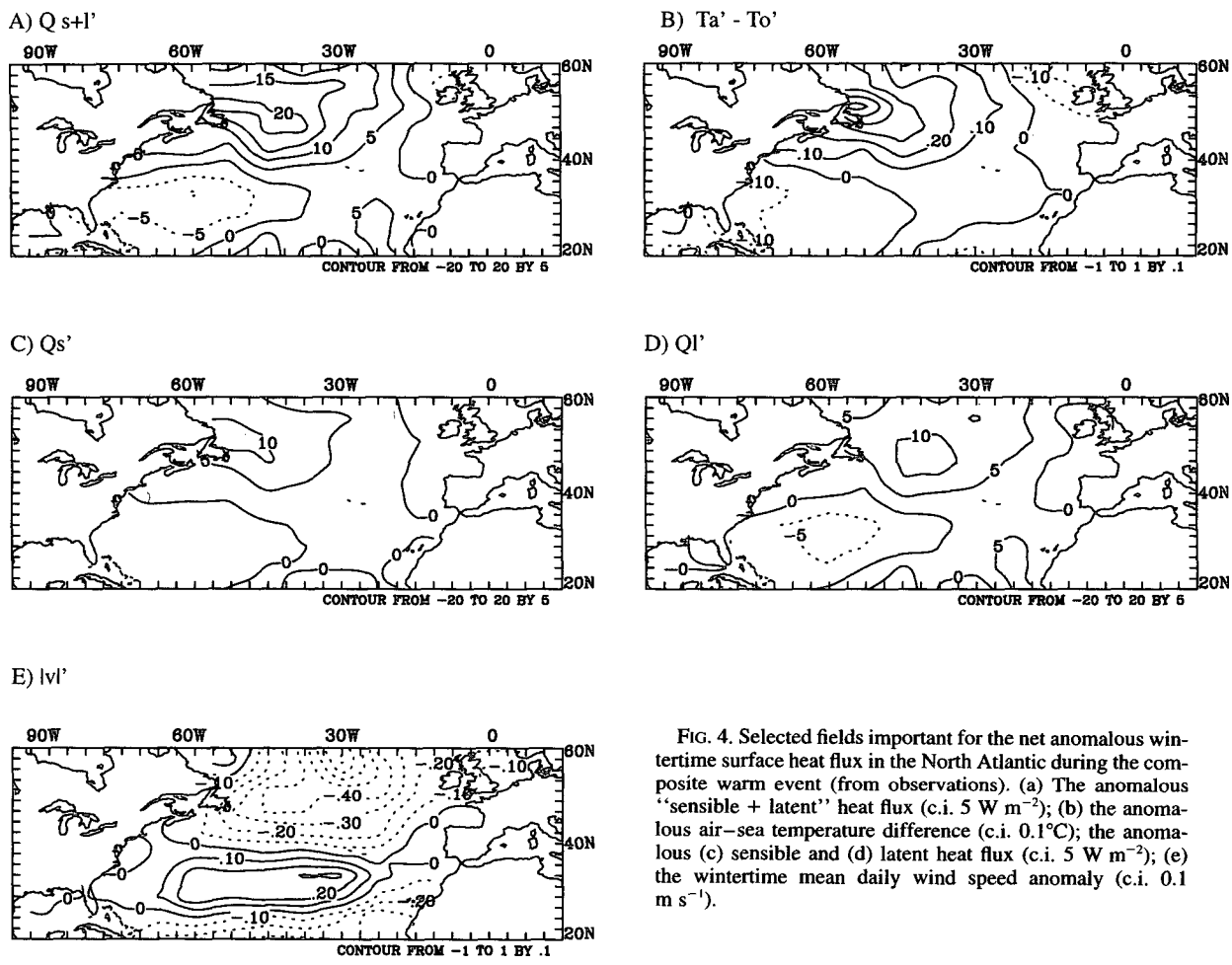

FIG. 4. Selected fields important for the net anomalous wintertime surface heat flux in the North Atlantic during the composite warm event (from observations). (a) The anomalous "sensible + latent" heat flux (c.i. 5 W m^{-2}); (b) the anomalous air–sea temperature difference (c.i. 0.1°C); the anomalous (c) sensible and (d) latent heat flux (c.i. 5 W m^{-2}); (e) the wintertime mean daily wind speed anomaly (c.i. 0.1 m s^{-1}).

39-yr control integration from that obtained in the hindcast. Similarly, surface Q_{S+L} flux anomalies are obtained by subtracting the net surface flux obtained in the 39-yr control integration (see section 2c) from that obtained in the hindcast integration:

$$Q_{\text{net}}(\text{hindcast}) - Q_{\text{net}}(\text{control}) = Q_{S+L}(\text{hindcast}) - Q_{S+L}(\text{control}) = Q'_{S+L};$$

Q_{net} is defined in Eq. (3).[3]

b. *The composite warm event*

Following Kushnir (1994), in Fig. 1 we present various composite surface fields from the warm phase of these interannual climate anomalies *observed* in the North Atlantic (see Table 1). The concomitant atmosphere and ocean variability depicted in Fig. 1 is consistent with Kushnir's interannual anomaly pattern[4] and with the "dipole mode" discussed in Deser and Blackmon (1993). In each of the simulated and observed composite fields that appears in the following figures, the anomalies that define the dipole structure are significant at or above the 95% confidence level.

The composite warm event from the observations (Fig. 1a) features warm water throughout most of the domain, except in the southwestern quadrant extending off the southeast United States where the SST anomalies are negative (−0.2°C). The warm anomalies are centered off the east coast of Canada with SST amplitude exceeding about +0.3°C. The spatial structure of the concomitant surface air temperature anomaly (cf. Figs. 1a,c) is very similar to the SST anomaly pattern.

[3] Note that the anomalies in the hindcast integration are not anomalies from the mean annual cycle of the control integration because the resultant anomalies would then include both the prescribed COADS signal and anomalies inherent to the CCM1 fields.

[4] The amplitudes of the composite fields presented in Fig. 1 and for the cold events (Fig. 6c) are less than that presented in Kushnir (1994) because of the application of the digital filter.

The observed air temperature anomalies are typically 50% to 100% greater than the SST anomalies in the center of both the warm and cold anomalies (cf. Figs. 1a,c and 4b). In the southern half of the domain, the anomalies in the surface air temperature are very similar in pattern to the SST anomalies, though only about 50% greater in amplitude.

The composite of the local surface Q_{S+L} heat flux anomalies, calculated from observations and shown in Fig. 4a, is largely consistent in pattern with the SST anomalies. Anomalous heating of the ocean is found coincident with the maximum SST anomalies and exceeds 20 W m^{-2}. The net heating anomalies are due to anomalies in both sensible and latent heating. Consistent with other studies (e.g., Alexander 1990; Cayan 1992a), these two components of heat flux are highly correlated (e.g., cf. Figs. 4c,d). South of about 35°–40°N, the latent heat flux is the dominant flux. North of this latitude, the sensible heat flux is almost comparable to the latent heat flux. In general, the pattern and sense of the heat flux anomalies and SST anomalies is consistent with the hypothesis that the SST anomalies result from a local interaction between the atmosphere and the oceanic mixed layer (Wallace and Jiang 1987; Alexander 1990; Wallace et al. 1990, 1992; Cayan 1992b).

The low-level atmospheric circulation that accompanies the warm composite is summarized in Figs. 1b,d, and 4e. Anomalously high (low) SLP is found in the northern (southern) half of the domain and the overall pattern has a dipole structure. A more complete description of the observed atmospheric anomalies and their role in the net surface heat flux anomalies is deferred to section 4a.

The composite warm event simulated by the ocean model is obtained by averaging the same years from the hindcast integration that went into the observed composite warm event (see Table 1). The simulated composite warm event is summarized in Fig. 5. In general, the SST anomalies from the ocean model are quantitatively consistent with those in the observed composite warm event (cf. Figs. 5a and 1a). Positive anomalies exceeding 0.25°C are found in the northwestern portion of the domain, with negative anomalies in the southern half of the domain (exceeding in absolute value 0.20°C in the southwest). As in the observations, the sensible and latent heat anomalies are in phase throughout the domain. The patterns of latent and sensible heat anomalies from observations are similar to those from the simulation. In the northern half of the domain, the sensible heat anomalies are about equal to that of the latent heat anomalies, while in the subtropics, the latent heat anomalies are much greater than sensible. The pattern of the net Q_{S+L} anomalies from the hindcast is similar to that "observed," albeit with weaker simulated fluxes in the northwestern domain (cf. Figs. 4a and 5e).

Typically, the mixed layer (Fig. 5g) is anomalously shallow (deep) where the SST anomalies are positive (negative) in the composite model warm event. The anomalous flux of heat into the mixed layer from below Q_e' (via changes in entrainment and convection) is displayed in Fig. 5f. Only in an isolated region in the far northwestern section of the domain (55°, 45°W) are the anomalies in the entrainment heat flux comparable to the net surface flux anomalies. Otherwise, anomalies in the entrainment flux are less than 40% of the anomalies in the net surface heat flux. Unfortunately, on the basin scale there are insufficient observations to estimate the actual anomalies in either the mixed layer depth (from XBTs) or the subsurface heat flux anomalies to the surface layer. Finally, it is interesting to note, in general, entrainment reinforces the negative surface flux anomalies in the subtropics and damps the positive anomalies in the northern part of the domain.

c. The composite cold event

The observation-based composite cold event features cold water throughout most of the northern half of the basin (Fig. 6c). The maximum negative SST anomaly exceeds −0.4°C and is located in the northwestern part of the basin. As in the warm event, the pattern of the air temperature anomalies is similar to the SST anomalies: the atmosphere minus ocean temperature difference is, typically, half of the SST anomaly (not shown).

The net surface heat flux anomalies that accompany the composite cold event from observations are displayed in Fig. 6a. Negative heat flux that cools the ocean is found in the northern half of the domain and is consistent with the observed negative SST anomalies. There exists a region of anomalous warming of the subtropical ocean, centered upon 30°N, 50°W. Along the northeast U.S. seaboard, however, the observed fluxes are cooling the ocean locally where anomalously warm water is found (see Figs. 6a,c). Throughout the domain in the cold composite event, the latent heat flux anomalies are in phase with the sensible heat flux anomalies (not shown). As in the warm composite event, both flux components contribute importantly to the net heat flux anomalies in the northern half of the domain, while the latent fluxes are about triple the sensible fluxes in the subtropics because of larger moisture capacity associated with the warmer air (see also Alexander 1990). The observation-based cold composite anomalies of SLP and surface wind are quantitatively similar to the negative of their counterparts from the warm case composite and, thus, are not shown.

The SST anomaly for the composite cold event from the hindcast integration is displayed in Fig. 6d. Overall, the simulated and observed cold composite SST anomalies are in good agreement in the northern half of the domain (cf. Figs. 6c,d). In the southwestern corner of

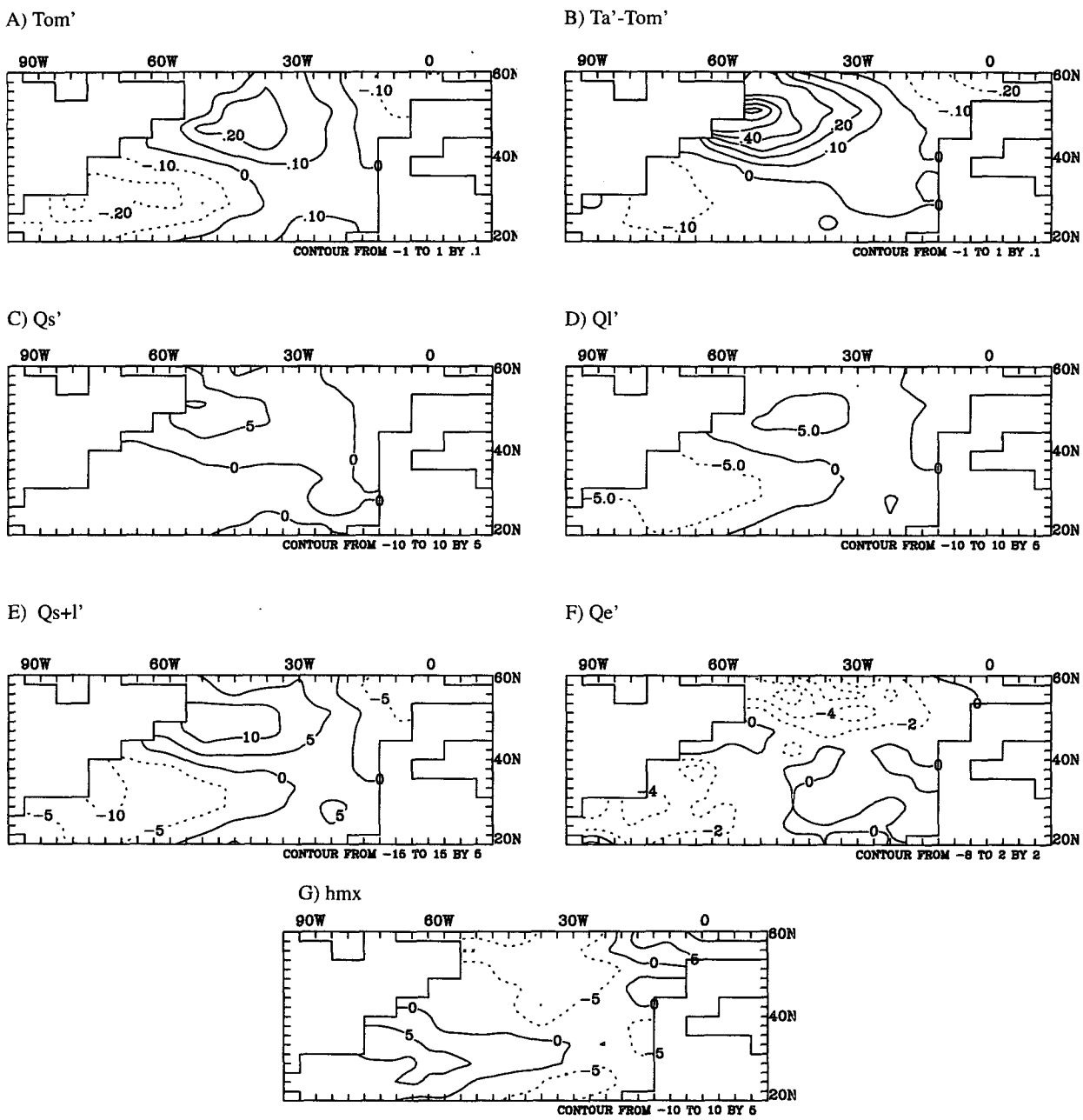

FIG. 5. A composite of wintertime (November to April) interannual "warm" events in the North Atlantic as simulated by the upper-ocean model. (a) SST (T'_{om}) anomaly (c.i. 0.1°C). (b) The anomalous air–sea temperature difference ($T'_a - T'_{om}$; c.i. 0.1°C). The anomalous fluxes of heat (c.i. 5 W m^{-2}) into the ocean mixed layer: (c) sensible Q'_S, (d) latent Q'_L, (e) "sensible + latent" Q'_{S+L}, and (f) entrainment Q'_e. Positive represents a heat gain in the mixed layer. (g) The anomalies in the mixed layer depth h (c.i. 5 m; solid contours for thicker mixed layer).

the domain the simulated warming is only about one half of the observed warming. As in the warm composite event, in the northern half of the domain the anomalies in "surface air temperature minus SST (or Tmix)" are about half that of the anomalies in SST (not shown). The pattern and amplitude of the individual (not shown) and net surface heat flux anomalies simulated by the model are, overall, consistent with those observed (cf. Figs. 6a,b). As in the simulated composite warm event, the mixed layer depth is anomalously shallow (deep) where the surface ocean is anomalously warm (cold) (not shown). Also, for the cold event, the wintertime (6-month average) anomalies in the subsurface fluxes into the mixed layer (Fig. 6e) are

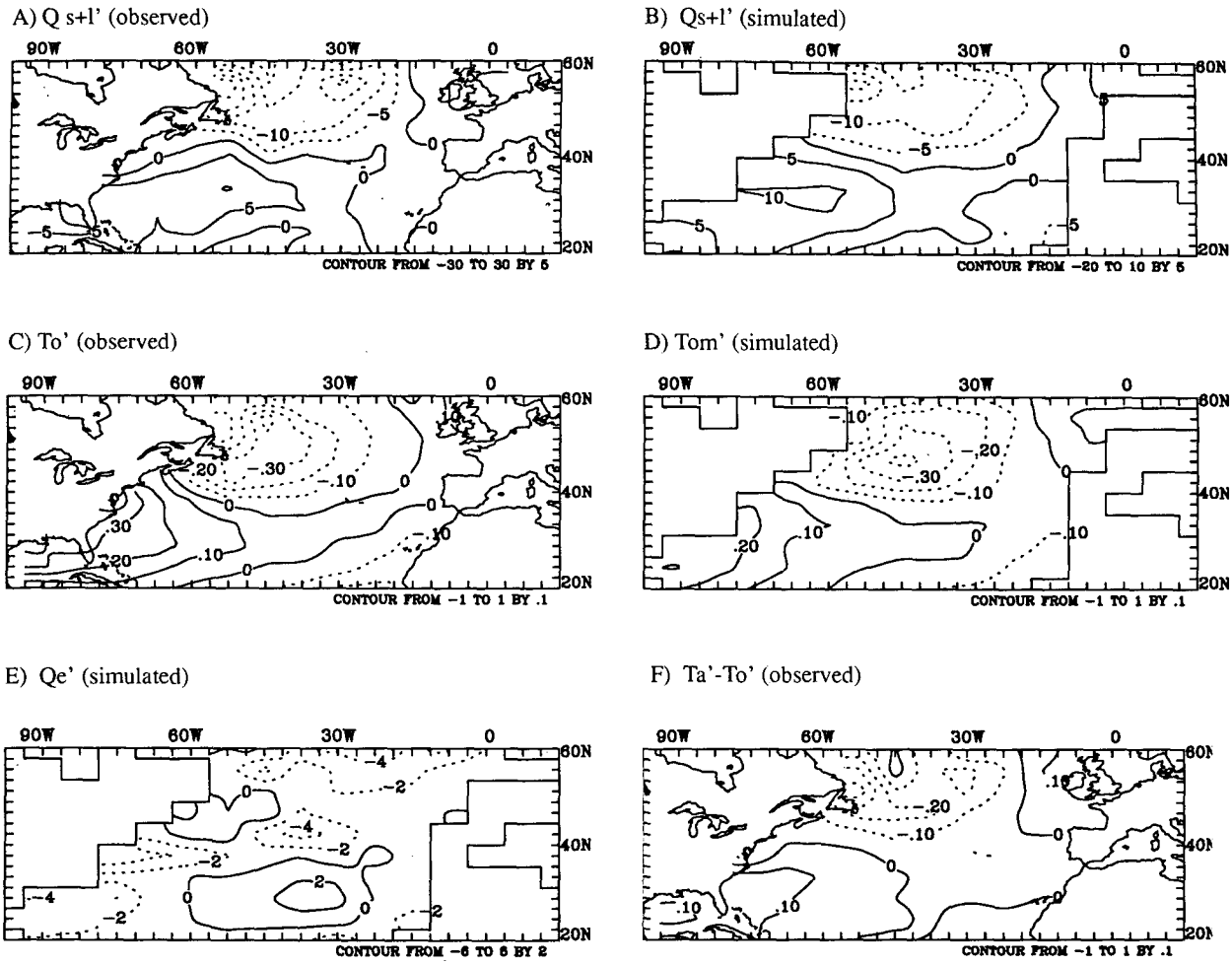

FIG. 6. Selected fields for the composite cold event. The anomalous "sensible + latent" heat flux from (a) observations and (b) simulations (c.i. 5 W m^{-2}). The anomalous SST from (c) observations and (d) simulation (c.i. is 0.1°C). (e) Simulated entrainment Q'_e anomaly (c.i. 5 W m^{-2}). (f) The observed anomalous air–sea temperature difference ($T'_a - T'_o$).

generally small (~25%) compared with the anomalies in the net (sensible plus latent) surface heat flux, though for about 2 months during early autumn the heating anomalies due to anomalous entrainment are larger than the anomalies in the net surface flux (Q_{S+L}).

4. Sensitivity studies

a. The role of varying surface air temperature, humidity, and wind speed

In this section we repeat the hindcast experiment of section 2, using only selected atmospheric fields in calculating the forcing. Recall that the heat flux anomalies in the hindcast of section 2 result from the prescribed (observed) monthly mean anomalies in surface air temperature, humidity, and daily mean wind speed. We report the results from three additional hindcast integrations. In the first hindcast (NT), we prescribe only the observed anomalies in q_a and V_a; the air temperature is from the control integration ($T'_a = 0$). A second experiment (NQ) is performed whereby anomalies in T_a and V_a are prescribed and q_a is from the control integration ($q'_a = 0$). A third hindcast integration (NW) is performed setting $V'_a = 0$ and prescribing the observed monthly anomalies in T_a and q_a. As in the hindcast integration of section 3, the warm composite event is formed from each integration and is plotted in Fig. 7.

For the warm event composite, monthly mean anomalies in the monthly average of the instantaneous wind *speed* are seen to have a small effect on the simulated SST anomalies (cf. Figs. 7a,d). Specifically, changes in the mechanical working of the mixed layer and in the *efficiency* of the sensible and latent heat transfer lead to relatively small changes in the surface heat content. On the other hand, withholding the information on the anomalies in either T_a or q_a degrade the hindcast

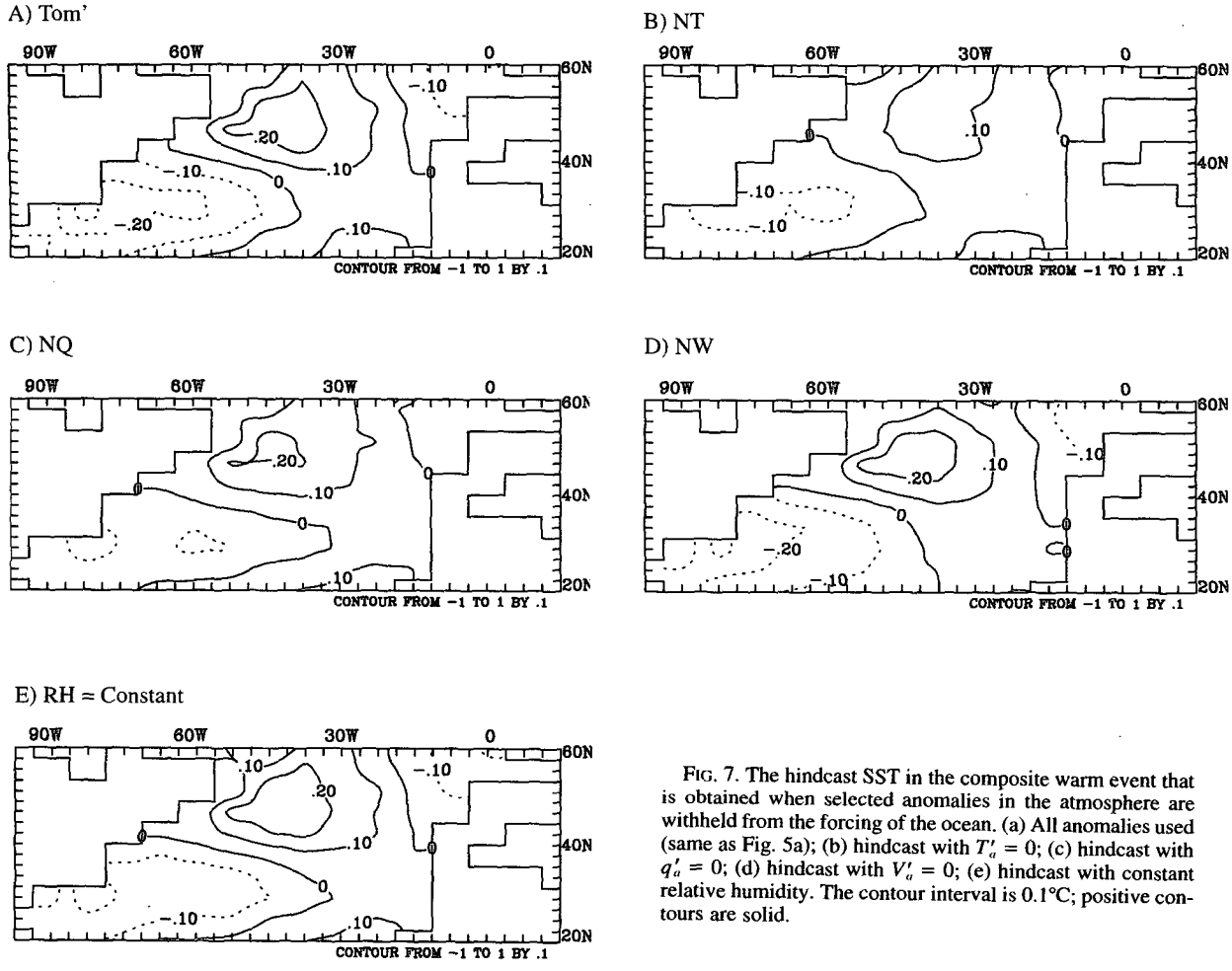

FIG. 7. The hindcast SST in the composite warm event that is obtained when selected anomalies in the atmosphere are withheld from the forcing of the ocean. (a) All anomalies used (same as Fig. 5a); (b) hindcast with $T_a' = 0$; (c) hindcast with $q_a' = 0$; (d) hindcast with $V_a' = 0$; (e) hindcast with constant relative humidity. The contour interval is 0.1°C; positive contours are solid.

significantly (cf. Figs. 7b,c with Fig. 7a). Note that changes in T_a and q_a are largely associated with changes in atmospheric advection. Results from the sensitivity studies NQ, NT, and NW using the cold case are similar to that from the warm case, and are not shown.

The sensitivity experiments NT and NQ examine independently the SST anomalies that result from the latent and sensible heat flux anomalies, respectively. It is often the case, however, that on the monthly timescale, the surface humidity adjusts with the surface temperature changes so as to maintain a constant relative humidity. Hence, another illuminating sensitivity study is to allow the air temperature anomalies in the hindcast but adjust the moisture anomalies so as to maintain a relative humidity that is instantaneously exactly the same as that in the control experiment. The result of this experiment (RH = constant) is shown in Fig. 7e for the warm case. Throughout most of the domain, the response is very similar to the full (TA) hindcast experiment (Fig. 7a), indicating the surface moisture adjusts rapidly with the intrusions of anomalously warm and cold air (rapidly compared with the timescale of the prescribed air temperature anomalies, 1 month). The southwest quadrant of the domain is the exception. In this region, cold air is associated with the advection of extremely dry continental air (Fig. 1d) and anomalies in relative humidity account for about half of the signal (cooling) in this region. The identical cold case RH = constant experiment shows that the anomalies in relative humidity account for only a small fraction of the anomalous heat flux throughout the domain, including in the southwest corner where, in the cold composite case, this region is anomalously warm.

b. *The composite hindcast events using prescribed flux anomalies*

In this section we obtain the composite warm and cold events using the same ocean model but now force the model with the net surface forcing anomalies Q_{S+L} that are estimated entirely from the observations of the

surface atmospheric fields and the *observed* SST: the flux anomalies are independent of the response of the ocean model. Hence, the composite formed from these integrations are referred to as "one-way forced" composites. For convenience, the hindcast of section 3b, which uses atmospheric fields and *simulated* SST in calculating the forcing, will be referred to as the partially coupled (PC) hindcast.

We proceed as follows. For each of the winters listed in Table 1 the "observed" flux anomalies are calculated from COADS using the bulk parameterization of Deardorff (1972). For each year that goes into the composite event (see Table 1), the "observed" monthly averaged Q_{S+L} flux anomalies are added to the net surface heat flux obtained from the ocean model control integration. The model is then integrated for 8 months, starting on 1 September for each year that goes into the warm and cold composite events: the initial conditions for the ocean temperature $T(z)$ are from the appropriate 1 September from the partially coupled hindcast. The composite warm (cold) event anomalies are then obtained by subtracting the model response from that obtained in the control run (described in section 2c) and averaging the individual warm (cold) events.

The "one-way forced (OWF) warm composite" SST and mixed layer depth anomalies are displayed in Figs. 8a,b. The spatial pattern of the OWF composite warm event is qualitatively similar to that from the PC hindcast integration and to that observed (cf. Figs. 8a, 5a, and 1a), though the OWF composite is somewhat noisier than that from either the observed or the PC hindcast composite. The notable differences between simulated and observed SST anomalies are found along the northeast U.S. coast, from Cape Hatteras to Nova Scotia (see the discussion in section 5). The amplitude of the warm anomaly centered in the northwestern part of the domain is about double that from the PC hindcast of section 3b. The pattern of the mixed layer depth anomalies in the PC hindcast is similar to that obtained in the OWF hindcast (cf. Figs. 8b and 5g), though the amplitude of the h anomalies are larger in the latter case (see Alexander 1992) because of the increase in the buoyancy anomalies due to larger SST anomalies in the OWF case.

The pattern of the entrainment anomalies in the OWF warm case (not shown) is very similar to that in the PC warm case (Fig. 5f). Thus, entrainment acts to dampen the warming in the northern domain. As in the PC case, the seasonally averaged (November–April) entrainment anomalies are less than 40% of the amplitude of the net heat flux anomalies. This is in contrast to the results presented in Alexander and Deser (1995), who show entrainment can contribute significantly to enhance SST anomalies during early fall.

There is a qualitative agreement between simulated and observed SST anomalies for the OWF cold case (not shown). Mixed layer depth anomalies are negative (shallow) in the southern domain and positive in the northern half of the domain, mainly due to changes in the buoyancy forcing. As in the warm case, the largest discrepancies between the OWF and the observed cold composite SST are found in a narrow strip of cold water along the northeastern U.S. seaboard from Cape Hatteras to Nova Scotia, where observations show warm anomalies but cold anomalies are simulated.

5. Discussion

Throughout most of the model domain, the hindcast OWF and PC composite warm and cold events are similar to their observed counterparts, indicating that interannual SST anomalies are explained largely by local surface heat flux anomalies. To estimate the amplitude of the SST anomalies that would be expected due to neglected advective effects on the *basinwide scale,* we performed a diagnostic calculation of the SST anomalies associated with the anomalous Ekman transport, calculated using the composite stress anomalies for the warm and cold composite events, estimated from COADS. Anomalies in SST associated with the anomalous Ekman advection are confined to north of 35°N and act to only modestly enhance the southern flank of the SST anomaly between 35° and 50°N in both the

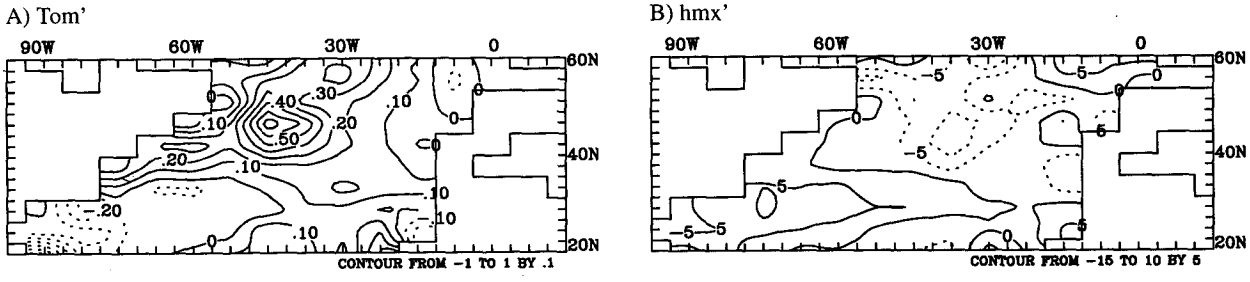

FIG. 8. A composite of wintertime (November to April) interannual warm events in the North Atlantic as simulated by the upper-ocean model, forced by the "observed" surface "sensible plus latent" heat flux anomalies. (a) SST (T'_{om}) anomaly (c.i. 0.1°C); (b) the anomalies in the mixed layer depth h (c.i. 5 m; solid contours for thicker mixed layer). The anomalous heat flux into the ocean mixed layer is plotted in Fig. 4a.

warm and cold case composite (consistent with the results presented in Luksch 1995). Hence, on a basin-wide scale, the amplitude of the advectively induced SST anomalies is small, being roughly 20% or less of the anomalies generated by the net surface heat flux anomalies. [Note along the U.S. eastern seaboard (in the western boundary current region) the current anomalies are due to both geostrophic and Ekman effects. Thus, the diagnostic calculations presented cannot provide an estimate of the advective impacts in this region.] The small contribution of the anomalous surface currents to the generation of interannual SST anomalies is also demonstrated in the results presented in Delworth (1995).

The region of largest disagreement between the simulated and observed SST anomaly is located in the wedge of ocean between Cape Hatteras and just south of Nova Scotia, extending offshore about one grid box (about 400 km). This region is exactly where the mean surface current is largest. The simulated SST anomalies for both the warm and cold composite OWF cases are of the *opposite* sign than is expected from the anomalies in the observed surface energy budget, indicating that in this localized region the atmospheric temperature anomalies are being forced *by* the oceanic anomalies. [The observed ocean temperature anomalies exceed air temperature anomalies (Fig. 6f). Thus, the net flux acts to damp the ocean temperature anomalies (cf. Figs. 6a,c).] The qualitative disagreement between the simulated and observed SST anomalies suggests that the SST anomalies in this region are due primarily to processes that are neglected in the model.[5] The neglected surface flux anomalies (e.g., radiation) are small compared with the anomalies Q_{S+L}. This region is, however, characterized by strong oceanic temperature gradients and ocean currents. Hence, it is likely that the dominant process for generating wintertime SST anomalies in this small region along the coast is advection in the ocean. Indeed, the SST anomalies along this narrow coastal strip could be explained by a mean northward advection of anomalous water, with the latter being a result of the anomalous surface flux forcing of the ocean in the southwestern part of the domain.

The weak dependence of the surface flux anomalies on the monthly mean anomalies in the daily wind speed $V_a \equiv |\mathbf{V}_a|$ is understood from the Taylor series expansion of the net heat flux:

$$Q'_S \propto \bar{V}_a(T'_a - T'_{om}) + V'_a(\bar{T}_a - \bar{T}_{om}) \quad (4)$$

$$-Q'_L \propto \bar{V}_a(q'_s - q'_a) + V'_a(\bar{q}_s - \bar{q}_a). \quad (5)$$

In Eqs. (4) and (5) the overbar denotes the monthly mean climatological value, the prime denotes the monthly mean anomaly, and the nonlinear terms have been neglected. Comparing the terms on the right-hand side in the North Atlantic basin, we find (typically)

$$\left|\frac{\bar{V}_a(T'_a - T'_{om})}{V'_a(\bar{T}_a - \bar{T}_{om})}\right| \sim \frac{10 \times 0.5}{1 \times 2}$$

$$= 2.5 \quad \text{and} \quad \left|\frac{\bar{V}_a(q'_s(T'_{om}) - q'_a)}{V'_a(\bar{q}_s(T_{om}) - \bar{q}_a)}\right| \sim \frac{10 \times 1}{1 \times 3} \sim 3.$$

The secondary role of the anomalous wind speed V'_a in generating SST anomalies in the midlatitudes was also noted by Haney et al. (1983), Cayan (1990), and Luksch and von Storch (1992).

The significant role of air temperature anomalies in generating SST anomalies was pointed out in section 4b. It is important to note that implicit in the prescribed air temperature anomaly T'_a is the process of atmospheric advection, specifically advection by high-frequency (unresolved) synoptic-scale eddies in the atmosphere. It is indeed likely that a large fraction of the monthly mean surface heat flux anomaly is, in general, due to the cumulative effect of horizontal advection of air with differing temperature and moisture by baroclinic eddies. [We note that a monthly mean anomaly in T_a and q_a could be attributed to synoptic events without observing a significant change V'_a.] It is likely, however, that prescribing the monthly mean atmospheric variables provides a reasonable estimate of the monthly mean surface flux attributed to the synoptic-scale storms (a related discussion is found in Trenberth et al. 1989).

It has been argued that by prescribing the atmospheric surface anomaly fields in concert with the bulk formulae representation for surface heat flux anomalies, the SST will be inextricably tied to the air temperature anomalies. To avoid prescribing the atmospheric fields Luksch and von Storch (1992) designed an advective atmosphere model of the (nondivergent) surface flow over the North Pacific. In their model, the observed climatological air temperatures at the edge of the model domain were prescribed, and the observed wind was prescribed to advect temperature as a tracer that experiences climatological damping and is influenced by the flux of sensible and latent heat to the ocean. The observed monthly mean winds are then imposed on the model. While the point of this model was to allow air temperatures to evolve more freely, it is puzzling that their sensitivity experiments (their section 5) did *not* indicate the heat flux anomalies were important in modifying the surface air temperature.

The coupling methodology (PC) we have used in section 3b ensures that *if* atmospheric circulation anomalies are indeed modified by the fluxes between the media, then a priori the observed atmospheric variables explicitly contain the effect of this forcing (see section

[5] Biases in the CCM climatological fields could introduce errors in the "observed" heat flux anomalies used in the OWF cases. This is not the case, however: we achieve very similar estimates for the net heat flux anomalies using only the COADS data and the Isemer and Hasse flux formulation (i.e., without reference to the CCM1 fields).

2). The methodology is thus identical to the experiments whereby SST anomalies are prescribed under an atmospheric GCM. Nonetheless, because the surface air temperature and SST anomalies closely track one another (e.g., cf. Figs. 1a and 4b) and the key fluxes (latent and sensible) for interannual climate fluctuations are strongly tied to the difference between air temperature and SST, it is possible that the simulated SST anomalies are overly constrained by the PC formulation of coupling. The good agreement between the OWF and observed composite warm and cold event SST anomalies somewhat alleviates this concern. However, to properly address the cause of the variability in the surface fields, and to allow for the possibility that the ocean affects the atmosphere, one must use a coupled atmosphere–ocean model. Indeed, presently we are analyzing experiments whereby the CCM1 has been coupled interactively to the North Atlantic Ocean model presented in this study. Preliminary results are presented in Bhatt et al. (1995) and will be discussed at length elsewhere.

Finally, we note the magnitude of the observed SST anomalies tend to be greater (less) than those in the PC (OWF) experiment. This indicates that the true negative feedback resulting from air–sea interaction lies in between the strong damping in the PC simulations and the absence of any feedback in the OWF simulations.

6. Conclusions

In this paper we examine the hypothesis that the interannual variability in wintertime North Atlantic SST is due to the variability in the surface heat flux, dominated by the variability in the sensible and latent heat flux. The hypothesis is tested by performing a hindcast integration of an upper-ocean model of the North Atlantic Ocean, forcing the model with surface heat and momentum fluxes calculated using the bulk formulae and the observed state of the atmosphere at the air–sea interface, from 1950 to 1988. The ability of the model to accurately hindcast the wintertime interannual variations in SST is demonstrated by simple correlations with the observed anomalies and, following Kushnir (1994), by comparing the composite of warm and cold events observed in the North Atlantic with those simulated by the model. The composite of SST, sensible, and latent heat flux anomalies from the observations are compared with those obtained from the ocean model hindcast. In addition, the entrainment and mixed layer depth anomalies from the ocean model hindcast are presented and discussed.

There is a good quantitative agreement between simulated and observed SST anomalies throughout most of the North Atlantic Ocean. Consistent with conclusions of other observational studies (e.g., Cayan 1992a,b), both sensible and latent heat flux anomalies are shown to contribute substantially to the wintertime anomalies in SST in the North Atlantic, while in the subtropics the heat flux anomalies are predominantly determined by the latent heat flux term. Entrainment anomalies contribute to a lesser extent to the mixed layer temperature anomalies throughout the domain (typically one-third or less of the net surface heat flux anomalies).

Since in the model formulation we explicitly exclude any effects due to *anomalies* in the ocean advection, our results confirm the hypothesis that wintertime interannual variability in the North Atlantic SST is mainly due to local anomalies in the air–sea flux of sensible and latent heat and not to anomalies in horizontal oceanic advection. There is significant disagreement between hindcast and observed SST anomalies only in a small region extending from Cape Hatteras to Nova Scotia along the U.S. coast. In this region, the observed surface flux anomalies are anticorrelated with the SST anomalies, implicating ocean advection as important for determining the interannual wintertime SST anomalies in a narrow region along the seaboard and, consequently, in *generating* surface flux anomalies. We note Haney (1985) and Miller (1992) found ocean current anomalies also play a secondary role ocean in generating interannual SST anomalies throughout the midlatitude Pacific Ocean (but contrast with Luksch 1995). Delworth (1995) came to a similar conclusion for the North Atlantic using a coupled atmosphere–ocean general circulation model.

Sensitivity studies are performed to highlight the variability in the atmosphere and the atmospheric processes that account for the surface heat flux anomalies. We find the anomalies in air temperature and humidity are fundamental to the net surface flux anomalies. The monthly mean anomaly in the monthly average of the instantaneous wind speed has little effect on either the surface fluxes or on the simulated SST anomaly.

The hindcast presented in this paper is a test of the ocean model, and is a necessary step in our ultimate goal: to examine the interaction between the ocean and the atmosphere in the midlatitudes and how this interaction affects circulation anomalies in the midlatitude atmosphere. Thus, the formulation in the coupling of the ocean to the atmosphere used in the hindcast of section 3 is designed to facilitate the next step: the interactive simulation using the ocean model and an atmospheric GCM. As a result, however, the heat fluxes that drive the ocean model depend on the difference between the atmospheric surface temperature and the simulated SST via the bulk formulae for the fluxes. To reassure the reader that the model response was not predetermined by this formulation of the coupling, we presented in section 4b the composite cold and warm events from the model when it was forced by the "observed" heat flux anomalies, estimated exclusively from COADS (using the bulk formulae and the observed interfacial fields), and independent of the response of the ocean model.

Do the observed SST anomalies, in turn, affect the atmospheric circulation? If so, how? The answers to these questions are not so clear. Numerous studies have suggested that, to varying degrees, midlatitude SST anomalies do affect the midlatitude atmospheric circulation (e.g., Palmer and Sun 1985; Pitcher et al. 1988; Lau and Nath 1990; Kushnir and Lau 1992; Miller 1992; Peng et al. 1995). We have initiated a series of experiments to further address this issue, coupling the CCM1 to the North Atlantic Ocean model used in the present study. Preliminary results have been obtained from two experiments: a 31-yr integration of the coupled global atmosphere–North Atlantic Ocean model, and the complementary control integration of the same atmosphere model forced with prescribed climatological SST from the coupled integration. These results indicate coupling *does* significantly modify the variability in the atmosphere over the North Atlantic domain (Bhatt et al. 1995).

Acknowledgments. We thank the two anonymous reviewers for insightful comments and suggestions that led to an improved presentation of these results. We are grateful for discussions with D. Houghton, B. Gallimore, and L. Keller concerning portions of this work. This work was funded by a grant from the NOAA Office of Global Change Programs and grants from the National Science Foundation (ATM-8913261 and ATM-9302884).

APPENDIX

Model Description

Following Niiler and Kraus (1977), the upper ocean in midlatitudes is represented by a well-mixed surface layer with uniform temperature and salinity and a sharp discontinuity in these quantities at the base of the mixed layer. Integrating the continuity equations for heat and salt over the mixed layer depth yields

$$\frac{\partial T_{om}}{\partial t} = w_e(T_b - T_{om})/h + \frac{(Q_{\text{tot}} - Q_{\text{SW}H})}{\rho_0 C_P h} + \frac{\nu_H}{h}\frac{\partial T_{om}}{\partial z}\bigg|_{z=h} \quad \text{(A1)}$$

$$\frac{\partial S_{om}}{\partial t} = w_e(S_b - S_{om})/h + \frac{S_{om}(E - P)}{\rho_0 h} + \frac{\nu_S}{h}\frac{\partial S_{om}}{\partial z}\bigg|_{z=h}, \quad \text{(A2)}$$

where T is the temperature, S salinity, t time, w_e the entrainment rate, h the mixed layer depth, ρ_0 the reference density, C_P the specific heat, z the vertical coordinate (positive down), E the evaporation rate, P the precipitation rate, $Q_{\text{SW}H}$ the penetrating solar radiation, and $\nu_H(\nu_S)$ the molecular diffusion coefficient for heat (salt). Subscripts *om* and *b* represent conditions within and below the mixed layer, respectively. The net *surface* heat flux is given by

$$Q_{\text{tot}} = Q_L + Q_S + Q_{\text{SW}} + Q_{\text{LW}_{\text{net}}}, \quad \text{(A3)}$$

where the fluxes are positive downward and Q_{SW} is the shortwave radiation, $Q_{\text{LW}_{\text{net}}}$ the net longwave radiation, and $Q_S(Q_L)$ is the sensible (latent) heat flux. The parameterizations used to compute the four components of Q_{net} are discussed in section 3b. The heat flux below the surface is due to penetrating solar radiation and is prescribed following Paulson and Simpson (1977):

$$Q_{\text{SW}H} = Q_{\text{SW}}(R\cdot\exp(-z/\xi_1) + (1 - R)\cdot\exp(-z/\xi_2)). \quad \text{(A4)}$$

The constants R, ξ_1, and ξ_2 depend on the optical water type (see Jerlov 1976) for which values over the North Atlantic have been obtained from Simonot and Le Treut (1986). At the base of the mixed layer, the water properties T_b and S_b are obtained directly from the layer in which h resides; below the mixed layer, temperature and salinity evolve according to

$$\frac{\partial T}{\partial t} = \frac{1}{\rho_0 C_P}\frac{\partial Q}{\partial z} + \nu_H\frac{\partial^2 T}{\partial z^2} \quad \text{(A5)}$$

$$\frac{\partial S}{\partial t} = \nu_S\frac{\partial^2 S}{\partial z^2}. \quad \text{(A6)}$$

There are two additional processes that influence the temperature and salinity within the model: convective overturning and an adjustment to conserved model properties. Convective adjustment occurs when the density of a layer exceeds the density of the layer below. The temperature of both layers is subsequently set to the mass-weighted mean. The conservation of heat, salt, and potential energy is ensured by adjusting T_{om} and T_b according to

$$T_{om} = T_{om} + \frac{(D_k - h - D_m)h(T_{om} - T_b)}{D_k D_m} \quad \text{(A7)}$$

$$T_b = T_b + \frac{(h - D_m)h(T_{om} - T_b)}{D_k(D_k - D_m)}, \quad \text{(A8)}$$

where $D_k = \Sigma_{l=1}^{k}\Delta z_l$ and $D_m = \max(h, D_k - \Delta z_k)$. Salinity is analogously adjusted.

The entrainment rate is derived from vertically integrating the turbulent kinetic energy equation over the mixed layer depth and then parameterizing the resulting terms using the known variables. The formula, common to most mixed layer models, can be expressed as follows:

$$w_e = \frac{mu_*^3 - 0.5hB(h) - h\epsilon}{q^2 + 0.5(h\Delta b - s\Delta \mathbf{v})}, \quad \text{(A9)}$$

where

$$B(h) = \frac{\alpha g}{\rho_{\text{ref}} C_P}\left(Q_{\text{tot}} + Q_{\text{SW}H} - \frac{2}{h}\int_0^h Q dz\right) + \frac{\beta g S_m}{\rho}(P - E) \quad \text{(A10)}$$

$$\Delta b = \alpha g \Delta T - \beta g \Delta S: \quad \text{(A11)}$$

$\Delta = \{\,|\,(\quad)_{om} - (\quad)_b\,|\,\}$ represents the discontinuity at the base of the mixed layer, u_* the friction velocity, ϵ the turbulent dissipation rate, $\mathbf{v}$ the velocity, q^2 the mean turbulent kinetic energy, and m and s are constants determined from observations. The thermal expansion coefficients α and β are determined from the international equation of state for seawater. The three terms in the numerator of (A9) represent the effects of wind stirring, changes in the buoyancy due to surface fluxes and penetrating solar radiation, and the dissipation of energy within the mixed layer. The terms in the denominator of (A9) are the energy required to agitate entrained water and the buoyancy jump at the base of the mixed layer. The instability term resulting from the shear across the base of the mixed layer is not included due to the transient nature of this term. The mean turbulent kinetic energy is parameterized according to Kim (1976):

$$q = 9 \cdot \max(10^{-4}\ \text{m}^2\ \text{s}^{-2}, u_*^2). \quad \text{(A12)}$$

Dissipation is an important process in the mixed layer: several approaches have been used to parameterize this term (cf. Niiler and Kraus 1977; Garwood 1977; Gaspar 1988). We use the formulation of Gaspar, as his model is designed for use in extended integrations (i.e., for integrations longer than a season). In addition, the model with this formulation of entrainment simulates better the depth of the mixed layer in summer. When $w_e \geq 0$, $dh/dt = w_e$, and w_e in (A9) becomes a function of the mixed layer depth, the Monin–Obukov length, and the Ekman length scale. When the mixed layer shallows, h is solved iteratively until a balance is reached between the wind stirring and the net buoyancy forcing over the depth of the mixed layer.

Numerical methods, model constraints, and initial conditions

The prognostic equations for T_{om}, S_{om}, and h are solved using a fourth-order Runge–Kutta scheme, which requires information at only one previous time step. All prognostic model equations are integrated using a one-day time step. Below the mixed layer, the integration is a forward differencing scheme in time.

The mixed layer depth is constrained to be greater than 10 m and less than 850 m to ensure computational stability. While long-lived mixed layer depths less than 10 m are extremely rare in nature, there is the potential for the model to simulated such shallow mixed layers in summer, as there are processes that act to keep the mixed layer away from the surface (e.g., surface wave mixing) that are not included in the model. In the hindcast integrations presented in section 3 of this paper, the mixed layer is initialized with the climatological values of T and S from Levitus (1982).

REFERENCES

Adamec, D., R. L. Elsberry, R. W. Garwood, and R. L. Haney, 1981: An embedded mixed-layer-ocean model. *Dyn. Atmos. Oceans,* **6,** 69–96.

Alexander, M. A., 1990: Simulation of the response of the North Pacific Ocean to the anomalous atmospheric circulation associated with El Nino. *Climate Dyn.,* **5,** 53–65.

——, 1992: Midlatitude atmosphere–ocean interaction during El Niño. Part I: The North Pacific Ocean. *J. Climate,* **5,** 944–958.

——, and C. Deser, 1995: A mechanism for the recurrence of wintertime midlatitude SST anomalies. *J. Phys. Oceanogr.,* **25,** 122–137.

Alexander, R. C., and R. L. Mobley, 1976: Monthly average sea-surface temperature and ice-pack limits in a 1° global grid. *Mon. Wea. Rev.,* **104,** 143–148.

Bhatt, U. S., M. A. Alexander, and D. S. Battisti, 1995: Coupled atmosphere–ocean climate variability in the North Atlantic. *Proc. of the 19th Climate Diagnostic Workshop,* College Park, MD, NOAA, 263–266.

Bjerknes, J., 1964: Atlantic air–sea interaction. *Adv. Geophys.,* **20,** 1–82.

Cayan, D. R., 1990: Variability of latent and sensible heat flux over the oceans. Ph.D. dissertation, University of California, San Diego, 199 pp. [Available from University of California, San Diego, MC A-024, La Jolla, CA 92093.]

——, 1992a: Variability of latent and sensible heat fluxes estimated using bulk formulae. *Atmos.–Ocean,* **30,** 1–42.

——, 1992b: Latent and sensible heat flux anomalies over the northern oceans: Driving the sea surface temperature. *J. Phys. Oceanogr.,* **22,** 859–881.

Davis, R. E., 1976: Predictability of sea surface temperature and sea level pressure anomalies over the North Pacific Ocean. *J. Phys. Oceanogr.,* **6,** 249–266.

Deardorff, J., 1972: Parameterization of the planetary boundary layer for use in general circulation models. *Mon. Wea. Rev.,* **100,** 93–106.

Delworth, T., 1995: North Atlantic interannual variability in a coupled ocean–atmosphere model. *J. Climate,* submitted.

Deser, C., and M. L. Blackmon, 1993: Surface climate variations over the North Atlantic Ocean during winter: 1900–1989. *J. Climate,* **6,** 1743–1753.

Garwood, R. W., 1977: An oceanic mixed layer model capable of simulating cyclic states. *J. Phys. Oceanogr.,* **7,** 455–468.

Gaspar, P., 1988: Modeling the seasonal cycle of the upper ocean. *J. Phys. Oceanogr.,* **18,** 161–180.

Haney, R. L., 1985: Midlatitude sea surface temperature anomalies: A numerical hindcast. *J. Phys. Oceanogr.,* **15,** 787–799.

——, B. H. Houtman, and W. H. Little, 1983: The relationship between wind and sea surface temperature anomalies in the mid-latitude North Pacific Ocean. *Atmos.–Ocean,* **21,** 168–186.

Isemer, H.-J., and L. Hasse, 1987: *The Bunker Climatic Atlas of the North Atlantic. Vol. 2: Air–Sea Interactions.* Springer-Verlag, 252 pp.

Jerlov, N. G., 1976: *Marine Optics.* Vol. 14, Elsevier Oceanogr. Ser., 231 pp.

Kim, J., 1976: A generalized bulk model of the oceanic mixed layer. *J. Phys. Oceanogr.,* **6,** 686–695.

Kushnir, Y., 1994: Interdecadal variations in North Atlantic sea surface temperature and associated atmospheric conditions. *J. Climate,* **7,** 141–157.

——, and N.-C. Lau, 1992: The general circulation model response to a North Pacific SST anomaly: Dependence on time scale and pattern polarity. *J. Climate,* **5,** 271–283.

Lanzante, J. R., 1984: A rotated eigenanalysis of the correlation between 700-mb heights and sea surface temperatures in the Pacific and Atlantic. *Mon. Wea. Rev.,* **112,** 2270–2280.

Lau, N.-C., and M. J. Nath, 1990: A general circulation model study of the atmospheric response to extratropical SST anomalies observed in 1950–79. *J. Climate,* **3,** 965–989.

Levitus, S., 1982: *Climatological Atlas of the World Ocean.* NOAA Prof. Paper 13. U.S. Govt. Printing Office, Washington DC, 173 pp.

Luksch, U., 1995: Simulation of North Atlantic low-frequency SST variability. *J. Climate,* submitted.

——, and von Storch, H., 1992: Modeling the low-frequency sea surface temperature variability in the North Pacific. *J. Climate,* **5,** 893–906.

Miller, A. J., 1992: Large-scale ocean–atmosphere interactions in a simplified coupled model of the midlatitude wintertime circulation. *J. Atmos. Sci.,* **49,** 273–286.

Niiler, P. P., and E. B. Kraus, 1977: Modeling and prediction of the upper layers of the ocean. *One-Dimensional Models of the Upper Ocean,* E. B. Kraus, Ed., Pergamon Press, 143–172.

Palmer, T. N., and Z. Sun, 1985: A modeling and observational study of the relationship between sea surface temperatures in the northwest Atlantic and the atmospheric general circulation. *Quart. J. Roy. Meteor. Soc.,* **111,** 947–975.

Paulson, C. A., and J. J. Simpson, 1977: Irradiance measurements in the upper ocean. *J. Phys. Oceanogr.,* **7,** 952–956.

Peng, S., L. Mysak, H. Ritchie, J. Derome, and B. Dugas, 1995: On the difference between early and middle winter atmospheric responses to sea surface temperature anomalies in the northwest Atlantic. *J. Climate,* **8,** 137–157.

Pitcher, E. J., M. L. Blackmon, G. Bates, and S. Munoz, 1988: The effect of North Pacific sea surface temperature anomalies on the January climate of a general circulation model. *J. Atmos. Sci.,* **45,** 173–188.

Sausen, R., and M. Ponater, 1988: Reducing the initial drift of a GCM. *Contrib. Atmos. Phys.,* **63,** 15–24.

Simonot, J.-Y., and H. L. Le Treut, 1986: Climatological field of mean optical properties of the World Ocean. *J. Geophys. Res.,* **91,** 6642–6646.

Soden, B. J., 1992: Validation of cloud forcing simulated by the National Center for Atmospheric Research Community Climate Model using observations from the Earth Radiation Budget Experiment. *J. Geophys. Res.,* **97,** 18 137–18 159.

Trenberth, K. E., W. G. Large, and J. G. Olson, 1989: The effective drag coefficient for evaluating wind stress over the oceans. *J. Climate,* **2,** 1507–1516.

van Loon, H., and J. C. Rogers, 1978: The seesaw in winter temperatures between Greenland and northern Europe. Part I: General description. *Mon. Wea. Rev.,* **106,** 296–310.

Wallace, J. M., and Q. Jiang, 1987: On the observed structure of the interannual variability of the atmosphere/ocean climate system. *Atmospheric and Oceanic Variability,* H. Cattle, Ed., Roy. Meteor. Soc., 17–43.

——, C. Smith, and Q. Jiang, 1990: Spatial patterns of atmosphere–ocean interaction in the northern winter. *J. Climate,* **3,** 990–998.

——, ——, and C. S. Bretherton, 1992: Singular value decomposition of wintertime sea surface temperature and 500-mb height anomalies. *J. Climate,* **5,** 561–576.

White, W. B., and A. E. Walker, 1974: Time and depth scales of anomalous subsurface temperature at ocean weather stations P, N, and V in the North Pacific. *J. Geophys. Res.,* **79,** 4517–4522.

Williamson, D. L., J. T. Kiehl, V. Ramanathan, R. E. Dickinson, and J. J. Hack, 1987: Description of NCAR Community Climate Model (CCM1). NCAR Tech. Note NCAR/TN-285+STR, 112 pp. [NTIS PB87-203782/AS.]